Nanotechnology

PAPER

Steep-slope field-effect transistors with AlGaN/GaN HEMT and oxide-based threshold switching device

IOP Publishing Nanotechnology
Nanotechnology 30 (2019) 215201 (7pp) https://doi.org/10.1088/1361-6528/ab0484

Steep-slope field-effect transistors with AlGaN/GaN HEMT and oxide-based threshold switching device

Xuanqi Huang[1], Runchen Fang[1,2], Chen Yang[1], Kai Fu[1], Houqiang Fu[1], Hong Chen[1], Tsung-Han Yang[1], Jingan Zhou[1], Jossue Montes[1], Michael Kozicki[1], Hugh Barnaby[1], Baoshun Zhang[3] and Yuji Zhao[1]

[1] School of Electrical, Computer & Energy Engineering, Arizona State University, Tempe, AZ 85287, United States of America
[2] Western Digital Corporation, 951 SanDisk Dr, Milpitas, CA, 95035, United States of America
[3] Key Laboratory of Nanodevices and Applications, Suzhou Institute of Nano-Tech and Nano-Bionics, Chinese Academy of Sciences, Suzhou 215123, People's Republic of China

E-mail: Yuji.Zhao@asu.edu

Received 4 December 2018, revised 28 January 2019
Accepted for publication 5 February 2019
Published 13 March 2019

Abstract

We report the demonstration of a steep-slope field-effect transistor with AlGaN/GaN MIS-HEMTs employing SiO_2-based threshold switching devices in series with the source. The SiO_2-based threshold switching devices exhibited steep slope when changing resistance states. The integrated steep-slope transistor showed a low subthreshold swing of sub-5 mV/dec with a transition range of over 10^5 in the transfer characteristics in both sweep directions at room temperature, as well as the low leakage current (10^{-5} μA μm^{-1}) and a high I_{ON}/I_{OFF} ratio ($>10^7$). Moreover, with the SiO_2-based threshold switching devices we also observed a positive shift of threshold voltages of the integrated device. Results from more than 50 transfer characteristics measurements also indicate the good repeatability and practicability of such a steep-switching device, where the average steep slopes are below 10 mV/decade. This steep-slope transistor with oxide-based threshold switching devices can be further extended to various transistor platforms like Si and III–V and are of potential interest for the development of power switching and high frequency devices.

Keywords: gallium nitride, steep slope, Boltzmann limit, threshold switching, transistor

(Some figures may appear in colour only in the online journal)

Nowadays, the continuance of Moore's law has become quite stringent for semiconductor foundries due to the limits of physics and fabrications [1, 2]. Meanwhile, conventional Si based MOSFETs are facing the fundamental limitation of the subthreshold swing (SS) by Boltzmann's theory [3]. To keep providing faster computing systems for customers in future generation electronics, innovative materials and technologies have been explored extensively. These include III–V compounds [4], two-dimensional (2D) materials [5], topological insulators [6] and neural networks [7].

Recently, researchers proposed to employ tunneling FETs and integrate ferroelectric materials on gate of FETs to realize the steep subthreshold switching [8, 9]. However, the average SS of these devices was larger than 30 mV/decade, which is still unsatisfying. Another effort includes adopting graphene-based resistive switching device to achieve steep slope (sub-10 mV/decade) and low leakage current [10]. It is claimed that this filament transistor can be scaling down to sub-10 nm without sacrificing performance. Nonetheless, the repeatability and homogeneity still remain a critical challenge for such 2D material-based devices.

An alternative approach is to combine phase-change materials with conventional FETs to realize phase-FET or hyper-FET. The metal–insulator–transition (or Mott insulator)

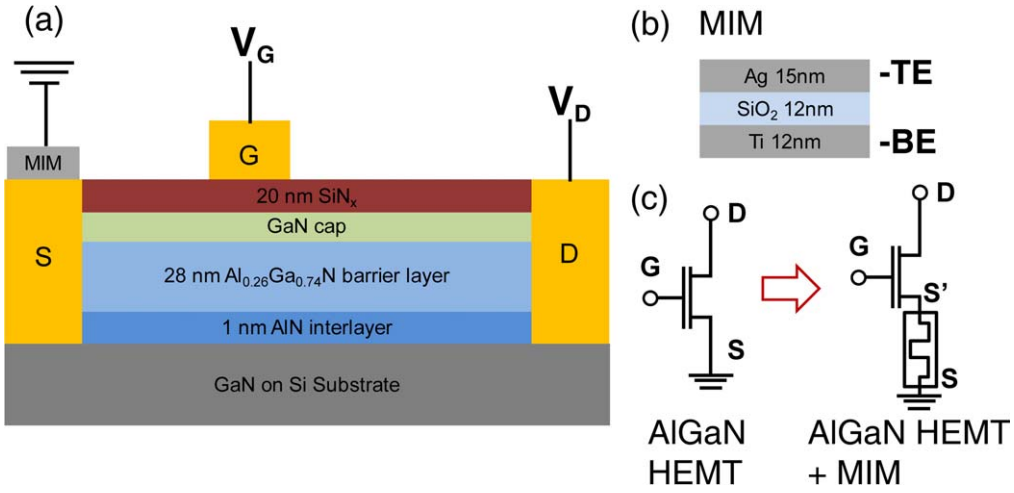

Figure 1. (a) Schematic cross-section view of the steep-threshold-switching AlGaN MIS-HEMT, (b) schematic structure of MIM used in this study and (c) schematic circuit diagrams of the stand-alone (left) and integrated steep-switching AlGaN MIS-HEMT device (right).

materials such as VO_2 and NbO_2 are commonly utilized on gate or source electrodes to obtain SS less than 8 mV/dec [11–13]. For example, a GaN-based phase-FET was demonstrated which integrated AlGaN/GaN MOS-HEMT with a VO_2 resistor [13]. Nonetheless, the claimed steep-switching occurred at the current saturation region in transfer characteristics and the SS at threshold voltages (V_{th}) has not been modulated by VO_2. In addition, Mott insulators suffer from thermal instability in high frequency applications. Another effort includes adopting threshold switching device based on Ag and Cu to achieve steep slope (sub-5 mV/decade) and low leakage current [14–16].

In this paper, we implemented SiO_2-based threshold switching device with the advanced AlGaN/GaN metal–insulator–semiconductor HEMTs (MIS-HEMTs) on Si substrates and demonstrated a steep-slope transistor (SST). Compared to Mott insulators, SiO_2 -based resistive random-access memory (RRAM) is favored primarily owing to the low leakage current and compatibility in the back-end-of-line (BEOL) processing in integrated circuits foundries [17–21]. This integrated SS-HEMT device achieved ~5 mV/dec SS with a transition range of over 10^5 in the transfer characteristics in both scan directions at RT. The V_{th} was also improved significantly. This SS-HEMT also inherited low leakage current ($\sim 10^{-5}$ μA μm^{-1}) and a high I_{ON}/I_{OFF} ratio ($>10^7$) from the original MIS-HEMTs. These results not only enable this novel transistor architecture to extend to other transistor systems, but also offer considerable possibilities for low-power switching and high frequency applications.

The AlGaN/GaN device epilayers for the MIS-HEMTs were grown by the metalorganic chemical vapor deposition on 2 inch Si substrates. Trimethylgallium (TMGa) and trimethylaluminum (TMAl) were used as the precursors for Ga and Al, respectively, and ammonia (NH_3) was the source for N. The carrier gas is H_2. As showed in figure 1(a), the heterostructure consists of a highly resistive GaN buffer layer grown on a Si substrate, a 100 nm GaN channel layer, a 1 nm AlN interlayer, a 28 nm $Al_{0.26}Ga_{0.74}N$ barrier layer, and a 2 nm GaN-cap layer. A 20 nm Si_3N_4 layer grown by low-pressure chemical vapor deposition (LPCVD) serves as the gate dielectrics and a passivation layer. The LPCVD-grown Si_3N_4 layer was deposited at 780 °C with ammonia (NH_3) flow of 280 sccm, a SiH_2Cl_2 flow of 70 sccm, and a deposition rate of 3.5 nm min^{-1} [22].

The AlGaN/GaN HEMTs were fabricated using the conventional photolithography. The wafer was cleaned in acetone and isopropyl alcohol under ultrasonic, and then dipped briefly in hydrochloric acid before metal depositions. Planar device isolation was achieved by multi-energy fluorine-ion implantation [23]. The LPCVD- Si_3N_4 in the source/drain contacting area was etched away by reactive ion etching. Ohmic contacts for source and drain regions were formed by e-beam evaporation of Ti/Al/Ni/Au (20/130/50/150 nm) and annealed at 890 °C for 30 s in N_2 ambient. Then gate metals were deposited by e-beam evaporation with Ni/Au (50/150 nmm) and lift-off process. The gate-to-source space, the gate-to-drain space, the gate width, and the gate length are 4, 15, 100, and 4 μm, respectively. After the MIS-HEMT fabrication, a 2D electron gas density of $\sim 1 \times 10^{13}$ cm^{-2} and electron Hall mobility of ~ 1800 cm^2 V^{-1} s^{-1} were measured at room temperature. More details on device fabrications can be found in references [23–26]. The circuit symbols for MIS-HEMT device denoting the source (S), gate (G) and drain (D) terminals are illustrated in figure 1(a).

Threshold switching devices with a metal–insulator–metal (MIM) structure were then fabricated on the source contacts of the MIS-HEMT, as showed in figure 1(a). Figure 1(b) shows the MIM structure including a 12 nm Ti bottom electrode (BE), a 12 nm SiO_2 switching layer and a 15 nm Ag top electrode, sequentially deposited by e-beam evaporation without interrupting the vacuum. Each MIM cell is circular with a diameter of 30 μm. No thermal annealing was conducted afterwards. The finial devices were denoted SS-HEMT. More details on the deposition and fabrication of SiO_2-based threshold switching cells can be found in [27]. DC characterizations of oxide-based threshold switching devices were carried out using a Keithley 2400 sourcemeter

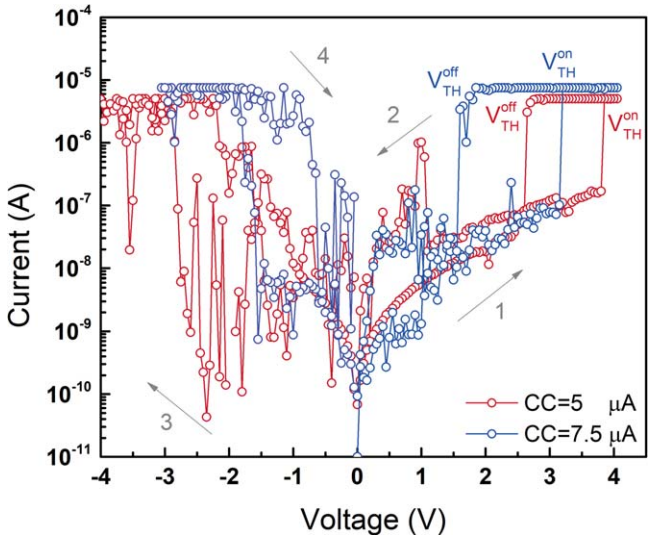

Figure 2. Representative current–voltage characteristics of the $Ag/SiO_2/Ti$ oxide-based threshold switching devices showing the resistive switching processes at current compliance of 5 μA (in red) and 7.5 μA (in blue). The scan sequence follows the labeled number: 1-2-3-4. 'V_{TH}^{on}' and 'V_{TH}^{off}' represent the threshold voltages of MIM device switching to 'ON' and 'OFF' states, respectively.

and transfer curves of the MIS-HEMTs and SS-HEMTs were performed using a Keithley 4200-SCS parameter analyzer. All measurements were performed at room temperature.

Figure 2 shows the representative resistive switching curves of the $Ag/SiO_2/Ti$ oxide-based threshold switching devices at two different current compliances (I_{CC}) of 5 μA (in red) and 7.5 μA (in blue). The scan was taken at a sequence of 1-2-3-4, as labeled in the figure 2. For each current compliance, ~30 cycles were conducted to ensure the device repeatability and endurance. Threshold switching devices will go from a high resistance state (HRS) to a low resistance state (LRS) or 'ON' state at a threshold voltage (V_{th}). All V_{th} values are marked in the figure 2. For $I_{CC} = 7.5$ μA, V_{TH}^{on} are ~3.7 V for positive scans and ~−1.8 V for negative scans. In contrast for $I_{CC} = 5$ μA, V_{TH}^{on} are ~3.2 V and ~−2.8 V. In addition, the ON state switched back to OFF state when the voltage sweeps back to a low level (V_{TH}^{off}= 1.5 V for $I_{CC} = 7.5$ μA and $V_{TH}^{off} = 2.5$ V for $I_{CC} = 5$ μA). The rectifying ratio of $\sim 10^2$ can be further enhanced with smaller MIM devices due to the inverse proportional relation between HRS and device size [16]. The device performance can be improved by reducing surface roughness of source electrodes and optimizing fabrication process. The possible threshold switching mechanism is proposed as the formation of unstable or even discontinuous conductive filaments at low compliance currents. More details on resistive switching mechanisms of the SiO_2-based threshold switching devices can be found in [28, 29].

Figure 3(a) illustrates the I_D–V_{GS} transfer characteristics of the stand-alone AlGaN/GaN MIS-HEMTs at drain voltages (V_{DS}) from 3 to 9 V and gate voltages (V_{GS}) from −14 to 4 V in both linear and logarithmic scales. The threshold voltage for HEMT (V_{th}), defined as the voltage at a current of 10^{-2} μA μm^{-1}, was determined as −12.28 V at a V_{DS} of 6 V in the forward scan. In addition, the hysteresis of V_{th} values between forward and backward scans is also obtained from figures 2(b) and (c). The hysteresis of V_{th} (ΔV_{th}) is defined by the following equation: $\Delta V_{th} = V_{th}$ (backward) − V_{th} (forward). The ΔV_{th} can originate from the acceptor-like trap states in the Si_3N_4/GaN interface [30, 31]. At $V_{DS} = 6$ V, a low ΔV_{th} of 0.22 V was observed due to a high quality interface between GaN and Si_3N_4 grown by LPCVD [23]. It is also noteworthy that hysteresis ΔV_{th} has a tendency to reduce as V_{DS} increases. This can be ascribed to the fact that fewer electrons would be captured by those aforementioned trap states when V_{DS} increases and then the electrical stress between gate and drain (V_{GD}) reduces. The saturation drain current (I_D) at $V_{GS} = 4$ V and $V_{DS} = 9$ V is 515 μA μm^{-1}. The ON/OFF ratio of over 10^7 was also achieved in this stand-alone AlGaN MIS-HEMT device.

Figures 3(b) and (c) show the I_D–V_{GS} transfer characteristics of integrated SS-HEMT at V_{DS} from 5 to 10 V for both forward scans and backward scans in logarithmic scales. The steep-subthreshold-switching behaviors were clearly observed in both scan directions. This steep slope switching occurs at a huge current range from ~10^{-5} μA μm^{-1} to more than 10^2 μA μm^{-1}, indicating a high ON/OFF ratio of more than 10^7. This large current transition range of over 7 decades is 100 times greater than previous report on Ag/TiO_2-Based steep-slope transistor [32]. All subthreshold-switching values are below 5 mV/dec. In addition, the drain current (I_D) was suppressed in the SS-HEMT compared to the stand-alone MIS-HEMT. This can be ascribed to the additional source resistance from the SiO_2-based threshold switching devices, leading to the reduction of the actual bias applied on the drain and thus the decrease of the drain current. For instance, at $V_{GS} = 3$ V and $V_{DS} = 9$ V, the drain current was 432 μA μm^{-1} for SS-HEMT device while it was 513 μA μm^{-1} for the stand-alone MIS-HEMT. This suppressed I_D phenomena is also consistent with previous reports on steep-slope transistors, such as AlGaN phase-FET with VO_2 [13], a Si MOSFET with NbO_2 on gate [11] and a Si MOSFET with atom switch devices based on Ag and Cu [16]. On the other hand, a positive shift in V_{th} values was observed in both scan directions compared to the standalone HEMT in figure 3(a). This trend is also consistent with previous work on steep-switching transistors [11–16, 32]. This shifting V_{TH} can be attributed to the intrinsic low leakage current and high resistance of SiO_2. SiO_2 has a huge bandgap of ~9.0 eV. This leads to the lower leakage current, larger current transition and smaller SS in our demonstrated steep-slope transistors. Once the threshold switching device is switched on, the integrated transistor will immediately rectify to the current saturation mode since the standalone HEMT is already turned on given the same gate voltage. In comparison, TiO_2 and other oxides typically have a relatively small bandgap between 3.0 and 6.0 eV. The leakage current or OFF current would be higher in transfer characteristics (I_D–V_{GS} measurements) and such steep-threshold-switching performance would be less pronounced if these oxides are adopted in our design. More details will be discussed in the later section.

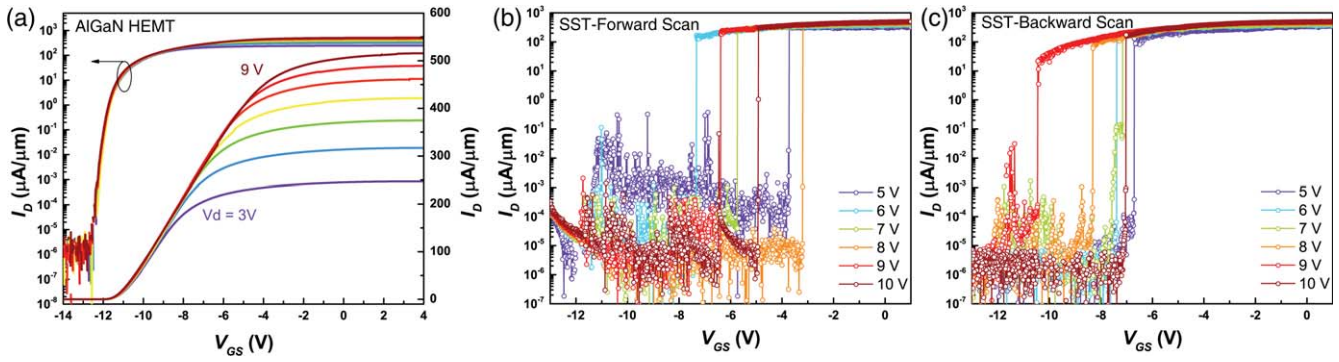

Figure 3. The I_D–V_{GS} transfer characteristics of (a) the stand-alone AlGaN/GaN MIS-HEMTs in both logarithmic (left) and linear (right) scales, and the integrated steep-slope AlGaN/GaN HEMTs (SS-HEMT) for (b) the forward scan and (c) the backward scan in logarithmic scales.

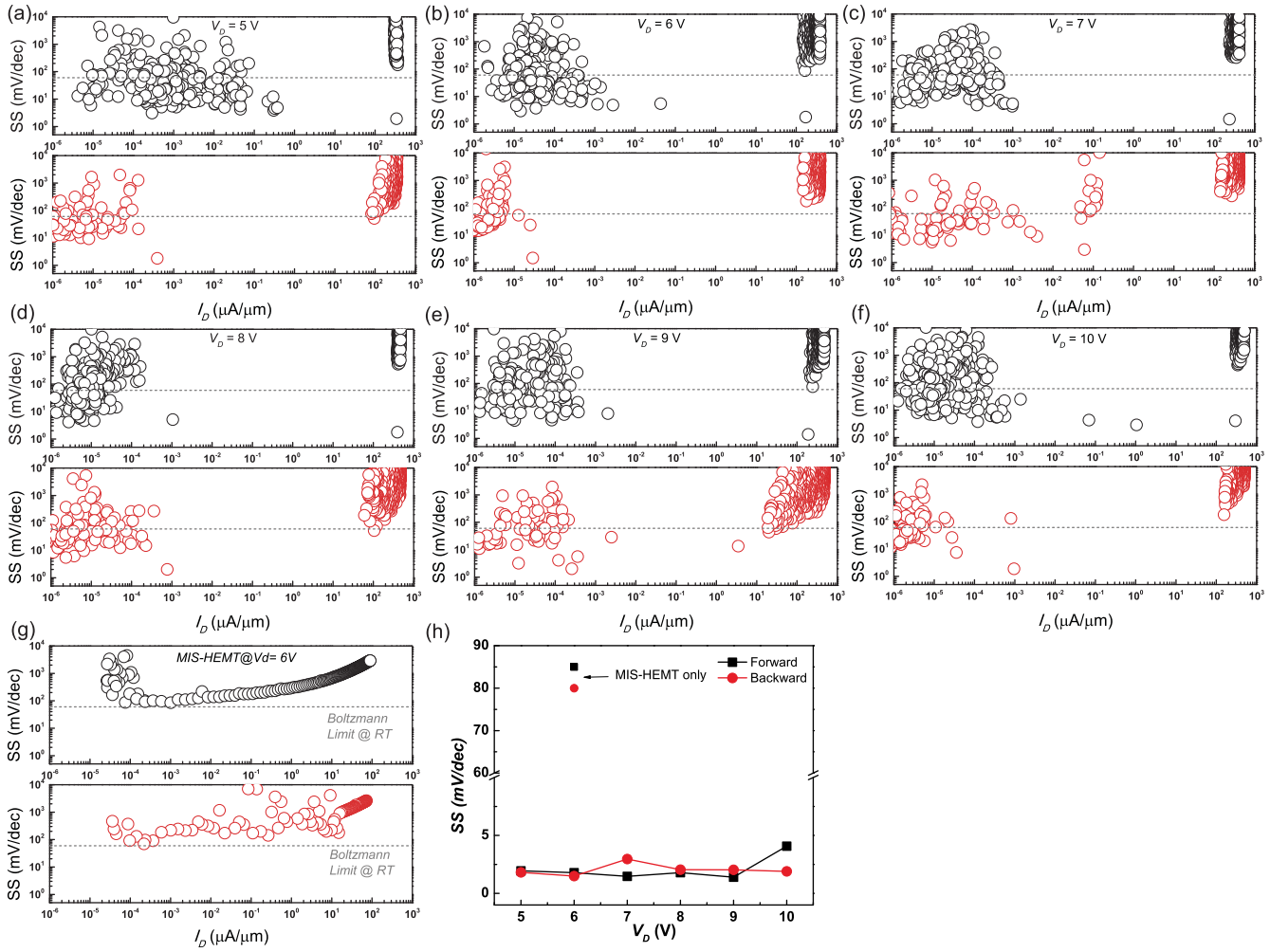

Figure 4. The extracted subthreshold swing (SS) as a function of the drain current (I_D) for the integrated steep-switching AlGaN/GaN HEMTs (SS-HEMTs) at V_{DS} = (a) 5 V, (b) 6 V, (c) 7 V, (d) 8 V, (e) 9 V and (f) 10 V, and (g) the stand-alone AlGaN/GaN MIS-HEMTs at V_{DS} = 6 V. (h) shows the summary of the SS values at a function of the applied drain voltages V_{DS} of the SS-HEMT and the stand-alone HEMT at V_{DS} = 6 V. All data displayed in black indicated the forward scan and the red for the backward scan. Grey dash lines indicate the subthreshold swing limit at room temperature for traditional transistor.

Figures 4(a)–(h) show the extracted SS as a function of the drain current for the integrated SS-HEMTs at V_{DS} = (a) 5 V, (b) 6 V, (c) 7 V, (d) 8 V, (e) 9 V and (f) 10 V in both scan directions, and (g) for the stand-alone AlGaN/GaN MIS-HEMTs at V_{DS} = 6 V. For the MIS-HEMT device, the SS values were much higher than the Boltzmann limit of 60 mV/dec at RT and the minimum values were ~ 85 mV/dec in the forward scan and ~80 mV/dec in the backward scan, respectively. With the integration of silica-based threshold switching devices, the steep subthreshold switching occurs at

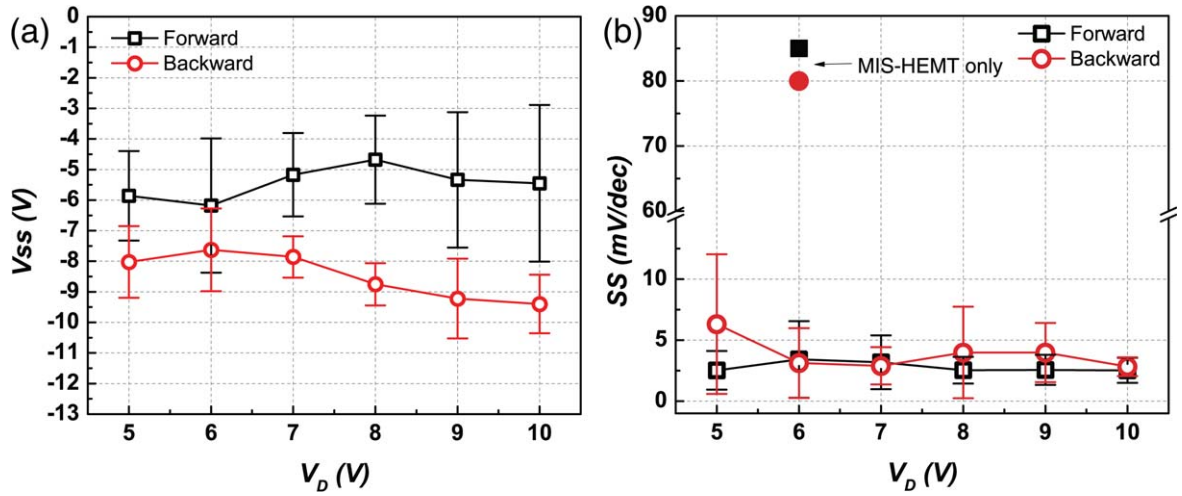

Figure 5. (a) Summary of V_{SS} values (defined as the gate voltage where the steep slope transition occurs) at a function of applied drain voltages V_{DS} of the SS-HEMT and (b) summary of SS values at a function of applied drain voltages V_{DS} of the SS-HEMT. SS values of the stand-alone HEMT at $V_{DS} = 6$ V are also plotted for reference.

an abrupt transition range of drain current, which is higher than 5 orders of magnitude in forward scans (see figures 4(a)–(f)). Figure 4(h) shows the summary of SS values at a function of applied drain voltage V_{DS}. Starting from $V_{DS} = 5$ V, the SS-HEMT exhibited the steep-subthreshold-switching behavior and dropped dramatically to 1.94, 1.79, 1.47, 1.47, 1.40 and 4.07 mV dec^{-1} at $V_{DS} = 5$, 6, 7, 8, 9 and 10 V in the forward scans. In backward scans, SS values were still far smaller than the Boltzmann limit of 60 mV dec^{-1} at RT, i.e. 1.81 mV/dec, 1.49 mV/dec, 2.96 mV dec^{-1}, 2.04 mV dec^{-1}, 2.02 mV dec^{-1} and 1.90 mV/dec at $V_{DS} = 5$ V, 6 V, 7 V, 8 V, 9 V and 10 V, respectively. It is worth pointing out that in the steep-slope ranges, SS values are comparable in both scan directions. However, this is not a general case for measurement results of more than 50 times. SS values in backward scans are generally larger than in the forward scans, which has previously been observed in the steep-switching AlGaN phase-FET with VO_2 [13]. This can be attributed to the fact that more electrons are accumulated in the SiO_2-based threshold switching devices during sweeping of V_{GS} from negative to positive range. Future work on characterizing the switching performance of this type of integrated AlGaN/GaN SS-HEMTs will be conducted to investigate the modulation capability.

In order to confirm the repeatability of the steep-slope HEMT device, we performed I_{DS}–V_{GS} measurements on multiple devices for more than 50 times. Summary of V_{SS} values (defined as the gate voltage where the steep slope transition occurs) at a function of applied drain voltages V_{DS} in the SS-HEMT and the summary of SS values at a function of applied drain voltages V_{DS} are shown in the figures 5(a) and (b), respectively. For each sweep direction of each drain voltages V_{DS}, more than 10 I_{DS}–V_{GS} curves were chosen to calculate the statistical distribution of V_{SS} and SS values. We can see that a positive shift in all subthreshold gate voltages where the steep slope transition occurs (V_{SS}) compared to those in a normal stand-alone HEMT device (~ -12.5 V). In addition, V_{SS} in backward scans are generally more negative than these in forward scans. This can be accounted for electron accumulation in both MIM and HEMT devices during sweeps. As for SS ranges shown in figure 5 (b), SS appears to be more stable at around 2–5 mV dec^{-1} as V_{DS} increases. Future work on achieving better stability of SS and device can be incorporating GaN-based threshold switching devices [24] and improving fabrication process.

The proposed threshold switching mechanisms are concluded as follows: with the SiO_2 threshold switching device on the source of a HEMT, the original gate voltage V_{GS} is composed of 2 parts: $V_{GS'}$ and $V_{S'S}$ (see figure 1(c)). The $V_{S'S}$ (<0V) is equal to the condition where Ag electrode was applied a positive voltage, namely $V_{SS'} > 0$, since this is a depletion-mode HEMT and steep switching occurs at a negative V_{GS}. There are three possible device operation scenarios:

(1) As $V_{GS} < V_{th}$ of HEMT [V_{th} (HEMT) ~ -12 V], the integrated HEMT behaves like a stand-alone HEMT and the device was turned off;
(2) As $V_{th} < V_{GS} < 0$, at a certain level of V_{GS}, $V_{S'S}$ will exceed the V_{th} of the SiO_2 threshold switching device [V_{th} (MIM)]. Then conductive filaments form between top and BEs. As the MIM device turns to LRS, the integrated transistor (HEMT in this case) will immediately rectify to the current saturation region and the steep switching occurs. This is due to the similar resistance states for both for SiO_2 MIM structure and HEMT since the OFF current is in the range from 10^{-9} to 10^{-7} A for SiO_2 MIM structure while the OFF current of HEMT is lower than 1×10^{-8} A (this is the detection limit of the setup-up).
(3) As V_{GS} sweep back, $V_{S'S}$ will exceed the V_{th} (MIM) at another certain level of V_{GS}. Then conductive filaments break, the MIM device turns to HRS, the steep switching occurs, and the transistor turns off.

In summary, we implemented the SiO_2-based threshold switching devices on the improved AlGaN/GaN MIS-HEMTs

on Si substrates and demonstrated a steep-slope transistor. This integrated SS-HEMT device achieved ~5 mV/dec SS with a current transition range of over 10^5 in the transfer characteristics in both scan directions at RT. It also inherited low leakage current ($\sim 10^{-5}$ μA μm^{-1}) and a high I_{ON}/I_{OFF} ratio ($>10^7$) from the MIS-HEMTs. Advantages of SiO_2-based threshold switching devices include intrinsic low leakage current, facile fabrication process, CMOS-compatible and controllable switching properties. Further engineering approaches can be adopted to fabricate the steep-slope transistor with desired switching behavior. For example, an enhancement-mode GaN HEMT, III–V transistors and even Si FinFETs can also be integrated with such SiO_2-based threshold switching devices. In addition, OFF current level can be further reduced by laterally scaling down the size of MIM structure. Therefore this novel transistor design harnesses the unique properties of facile and CMOS-compatible SiO_2-based threshold switching devices and promises numerous performance advantages over conventional three-terminal transistors.

Acknowledgments

This work is supported by ARPA-E PNDIODES Program monitored by Dr Isik Kizilyalli (Grant number DE-AR0000868) and partially supported by NASA HOTTech Program (grant number 80NSSC17K0768). The device fabrication was performed in Nanofab at Arizona State University. This work was supported, in part, by NSF award number NNCI–1542160.

ORCID iDs

Xuanqi Huang https://orcid.org/0000-0002-7085-4162
Houqiang Fu https://orcid.org/0000-0002-1125-8328

References

[1] Shilov A and Cutress I 2018 *GlobalFoundries Stops All 7nm Development: Opts To Focus on Specialized Processes* Anand Tech https://www.anandtech.com/show/13277/globalfoundries-stops-all-7nm-development
[2] Hruska J 2018 *Intel Won't Have 10 nm CPUs Ready Until the End of 2019* Extreme Tech https://www.extremetech.com/computing/274373-intel-wont-have-10nm-cpus-ready-until-the-end-of-2019
[3] Meindl J D, Chen Q and Davis J A 2001 Limits on silicon nanoelectronics for terascale integration *Science* **293** 2044–9
[4] Alamo J A del 2011 Nanometre-scale electronics with III–V compound semiconductors *Nature* **479** 317–23
[5] Radisavljevic B, Radenovic A, Brivio J, Giacometti V and Kis A 2011 Single-layer MoS_2 transistors *Nat. Nanotechnol.* **6** 147–50
[6] Kong D *et al* 2011 Ambipolar field effect in the ternary topological insulator $(Bi_xSb_{1-x})_2Te_3$ by composition tuning *Nat. Nanotechnol.* **6** 705–9
[7] Choi S, Tan S H, Li Z, Kim Y, Choi C, Chen P-Y, Yeon H, Yu S and Kim J 2018 SiGe epitaxial memory for neuromorphic computing with reproducible high performance based on engineered dislocations *Nat. Mater.* **17** 335–40
[8] Huang Q, Huang R, Zhan Z, Qiu Y, Jiang W, Wu C and Wang Y 2012 A novel Si tunnel FET with 36mVdec^{-1} subthreshold slope based on junction depleted-modulation through striped gate configuration *2012 Int. Electron Devices Meeting 2012 Int. Electron Devices Meeting* pp 8.5.1–4
[9] Salahuddin S and Datta S 2008 Use of negative capacitance to provide voltage amplification for low power nanoscale devices *Nano Lett.* **8** 405–10
[10] Tian H, Wang X, Zhao H, Mi W, Yang Y, Chiu P-W and Ren T-L 2018 A graphene-based filament transistor with Sub-10 mV dec^{-1} subthreshold swing *Adv. Electron. Mater.* **4** 1700608
[11] Park J, Lee D, Yoo J and Hwang H 2017 NbO2 based threshold switch device with high operating temperature (>85°C) for steep-slope MOSFET (~2mVdec^{-1}) with ultra-low voltage operation and improved delay time 2017 *IEEE Int. Electron Devices Meeting (IEDM) 2017 IEEE Int. Electron Devices Meeting (IEDM)* pp 23.7.1–4
[12] Shukla N, Thathachary A V, Agrawal A, Paik H, Aziz A, Schlom D G, Gupta S K, Engel-Herbert R and Datta S 2015 A steep-slope transistor based on abrupt electronic phase transition *Nat. Commun.* **6** 7812
[13] Verma A, Song B, Downey B, Wheeler V D, Meyer D J, Xing H G and Jena D 2018 Steep sub-boltzmann switching in AlGaN/GaN phase-FETs with ALD VO_2 *IEEE Trans. Electron Devices* **65** 945–9
[14] Song J, Woo J, Prakash A, Lee D and Hwang H 2015 Threshold selector with high selectivity and steep slope for cross-point memory array *IEEE Electron Device Lett.* **36** 681–3
[15] Song J, Park J, Moon K, Woo J, Lim S, Yoo J, Lee D and Hwang H 2016 Monolithic integration of AgTe/TiO_2 based threshold switching device with TiN liner for steep slope field-effect transistors *2016 IEEE Int. Electron Devices Meeting (IEDM) 2016 IEEE Int. Electron Devices Meeting (IEDM)* pp 25.3.1–4
[16] Lim S, Yoo J, Song J, Woo J, Park J and Hwang H 2016 Excellent threshold switching device (Ioff ~ 1 pA) with atom-scale metal filament for steep slope (<5mVdec^{-1}), ultra low voltage (Vdd = 0.25V) FET applications *2016 IEEE Int. Electron Devices Meeting (IEDM) 2016 IEEE Int. Electron Devices Meeting (IEDM)* pp 34.7.1–37.7.4
[17] Tappertzhofen S, Menzel S, Valov I and Waser R 2011 Redox processes in silicon dioxide thin films using copper microelectrodes *Appl. Phys. Lett.* **99** 203103
[18] Chen W, Barnaby H J and Kozicki M N 2016 Impedance spectroscopy of programmable metallization cells with a thin SiO_2 switching layer *IEEE Electron Device Lett.* **37** 576–9
[19] Chen W, Tappertzhofen S, Barnaby H J and Kozicki M N 2017 SiO_2 based conductive bridging random access memory *J. Electroceram.* **39** 109–31
[20] Lübben M, Menzel S, Park S G, Yang M, Waser R and Valov I 2017 SET kinetics of electrochemical metallization cells: influence of counter-electrodes in SiO_2/Ag based systems *Nanotechnology* **28** 135205
[21] Mehonic A *et al* 2018 Silicon oxide (SiOx): a promising material for resistance switching? *Adv. Mater.* 1801187
[22] Zhang Z *et al* 2016 Studies on high-voltage GaN-on-Si MIS-HEMTs using LPCVD Si_3N_4 as gate dielectric and passivation layer *IEEE Trans. Electron Devices* **63** 731–8
[23] Zhang Z *et al* 2017 AlGaN/GaN MIS-HEMTs of very-low V_{th} hysteresis and current collapse with *in-situ* pre-deposition plasma nitridation and LPCVD-Si_3N_4 gate insulator *IEEE Electron Device Lett.* **38** 236–9

[24] Fu K, Fu H, Huang X, Yang T, Chen H, Baranowski I, Montes J, Yang C, Zhou J and Zhao Y 2019 Threshold switching and memory behaviors of epitaxially regrown GaN-on-GaN vertical p–n diodes with high temperature stability *IEEE Electron Device Lett.* (https://doi.org/10.1109/LED.2019.2891391)

[25] Fu K *et al* 2018 Investigation of GaN-on-GaN vertical p-n diode with regrown p-GaN by metalorganic chemical vapor deposition *Appl. Phys. Lett.* **113** 233502

[26] Fu H *et al* 2018 Nonpolar vertical GaN-on-GaN p–n diodes grown on free-standing (10 $\bar{1}$0) *m* -plane GaN substrates *Appl. Phys. Express* **11** 111003

[27] Chen W, Fang R, Balaban M B, Yu W, Gonzalez-Velo Y, Barnaby H J and Kozicki M N 2016 A CMOS-compatible electronic synapse device based on $Cu/SiO_2/W$ programmable metallization cells *Nanotechnology* **27** 255202

[28] Chen W, Barnaby H J, Kozicki M N, Edwards A H, Gonzalez-Velo Y, Fang R, Holbert K E, Yu S and Yu W 2015 A study of gamma-ray exposure of $Cu–SiO_2$ programmable metallization cells *IEEE Trans. Nucl. Sci.* **62** 2404–11

[29] Valov I, Waser R, Jameson J R and Kozicki M N 2011 Electrochemical metallization memories—fundamentals, applications, prospects *Nanotechnology* **22** 289502

[30] Zhang Z *et al* 2016 Fabrication of normally-off AlGaN/GaN metal–insulator–semiconductor high-electron-mobility transistors by photo-electrochemical gate recess etching in ionic liquid *Appl. Phys. Express* **9** 084102

[31] Wu T, Franco J, Marcon D, Jaeger B D, Bakeroot B, Stoffels S, Hove M V, Groeseneken G and Decoutere S 2016 Toward understanding positive bias temperature instability in fully recessed-gate GaN MISFETs *IEEE Trans. Electron Devices* **63** 1853–60

[32] Song J, Woo J, Lee S, Prakash A, Yoo J, Moon K and Hwang H 2016 Steep slope field-effect transistors with Ag/TiO_2-based threshold switching device *IEEE Electron Device Lett.* **37** 932–4